Check for updates

Received: 20 May 2023 | Revised: 19 October 2023 | Accepted: 19 October 2023

DOI: 10.1002/app.54856

RESEARCH ARTICLE

Applied Polymer SCIENCE WILEY

Adsorption of uranium (VI) from aqueous solutions using boron nitride/polyindole composite adsorbent

Deniz Emre[1] | **Özlem Selçuk Zorer**[2] | **Ali Bilici**[3] | **Erhan Budak**[4] | **Selehattin Yilmaz**[3] | **Necla Caliskan Kilic**[2] | **Eda Gokirmak Sogut**[5]

[1]Vocational School of Health Services, Çanakkale Onsekiz Mart University, Çanakkale, Turkey

[2]Faculty of Science, Department of Chemistry, Van Yuzuncu Yil University, Van, Turkey

[3]Faculty of Sciences, Department of Chemistry, Çanakkale Onsekiz Mart University, Çanakkale, Turkey

[4]Faculty of Arts and Sciences, Department of Chemistry, Bolu Abant Izzet Baysal University, Bolu, Turkey

[5]Van Security Vocational School, Van Yuzuncu Yil University, Van, Turkey

Correspondence
Özlem Selçuk Zorer, Faculty of Science, Department of Chemistry, Van Yuzuncu Yil University, Van 65080, Turkey.
Email: selcukozlems@gmail.com

Ali Bilici, Faculty of Sciences, Department of Chemistry, Çanakkale Onsekiz Mart University, Çanakkale 17100, Turkey.
Email: alibilici66@hotmail.com

Funding information
Çanakkale Onsekiz Mart Üniversitesi, Grant/Award Number: FBA-2022-4033

Abstract

Turbostratic boron nitride (tBN) surface is modified with polyindole (PIn) by a facile polymerization technique and the uranyl adsorption efficiency of this mesoporous hybrid is investigated. The successful surface modification is confirmed by FT-IR, Raman, XRD, TEM, SEM, EDX, EDS mapping XPS, BET, and zeta potential techniques. The batch experiments are performed in various temperatures (T), contact times (t), pH, and initial solution concentrations (C_0) to evaluate its adsorption performance. The optimum adsorption performance is achieved at pH = 5.0–5.5, $T = 307$ K, $t = 10$ min, $C_0 = 18$ mg L^{-1}. These experimental results are evaluated using Freundlich, Redlich–Peterson, and Langmuir isotherm models, which presents equivalent regression coefficients. Maximum adsorption capacity (q_m) of the nanoadsorbent (tBN/PIn), determined by the Langmuir isotherm, is 315.29 mg g^{-1}. The adsorption kinetics of uranyl ions on tBN/PIn are in harmony with the pseudo-second order model. tBN/PIn nanoadsorbent provides high adsorption efficiency even at exceptionally low UO_2^{2+} concentration range (4–40 mg L^{-1}) and low adsorbent mass (0.005 g). XPS analysis results show that 0.05% of uranium is adsorbed on tBN/PIn via mainly U-O coordination. The results of present study demonstrate that tBN/PIn can a potential adsorbent for removing uranium from aqueous solutions.

KEYWORDS

adsorption, polyindole, turbostratic boron nitride, uranium, wastewater treatment

1 | INTRODUCTION

Uranium radionuclides are hazardous pollutants because of their high radioactivity and chemical toxicity.[1] The World Health Organization (WHO) allows maximum 30 μg L^{-1} of total uranium content in potable water.[2] Higher amounts of uranium can cause serious health issues and even death.[3] Therefore, uranium effluents must be adequately treated.[4] For this purpose, various separation and purification processes are used to remove uranium from wastewater. Some of these processes are precipitation,[5] adsorption,[6] biological treatment,[7] ion

This is an open access article under the terms of the Creative Commons Attribution-NonCommercial-NoDerivs License, which permits use and distribution in any medium, provided the original work is properly cited, the use is non-commercial and no modifications or adaptations are made.
© 2023 The Authors. *Journal of Applied Polymer Science* published by Wiley Periodicals LLC.

exchange,[8] and so on.[9] Amongst them, adsorption is a commonly preferred technique for water purification due to its high selectivity, ease of use, adaptability, recyclability, and environmental safety.[1,6] Numerous organic and inorganic materials including graphene, carbon nanotubes, activated carbon, metal organic frameworks,[10,11] polymers,[12] MXenes,[13] and their derivatives are utilized as effective adsorbents for water treatment research.[9,14] These adsorbents present both some advantages and disadvantages.[10] Therefore, there is still an increasing need and interest in development of these kind of effective adsorbent materials.

Boron nitride (BN), named as also white graphite, is a charming nanomaterial for the adsorption of uranium.[15] BN has various crystalline phases such as hexagonal-BN, cubic-BN, wurtzite-BN, amorphous-BN, and turbostratic BN (tBN).[16] The desired BN structure can be obtained by adjusting the synthesis conditions.[16] tBN has a semi-crystalline structure, and its two-dimensional hexagon layers are stacked in partly parallel positions with random rotations.[17]

Boron nitride nanomaterials have remarkable characteristics such as high thermal and mechanical strength, oxidation resistance, low density, and large surface area.[6,14] These properties make BNs preferred materials for hydrogen storage, protective coating, and gas purification applications.[6] BN-based materials are also used as effective adsorbents for heavy metal, dye, and organic compound removal.[6]

Application areas of BNs are expanded by their surface modification.[18] For example, various functional groups, such as amine, hydroxyl, acryl, and carboxyl, are attached to BN main skeleton for these purposes.[19] Another method for functionalizing of BN surface is to prepare its nanocomposites with functional polymers. Such a functionalization process improves the compatibility and dispersibility properties of the BN.[19,20] For instance, BN nanocomposites with polyaniline, and polyacrylic acid were prepared. These nanomaterials were effective adsorbents for removal of various pollutants.[21,22]

Conductive polymers are highly researched materials because they exhibit interesting physical and chemical characteristics that belong to both organic polymers and metals. Studies are particularly focused on nitrogen-containing heterocyclic conductive polymers such as polypyrrole, polyaniline and their derivatives.[23] PIn is a member of heterocyclic conductive polymers and has an aromatic structure consisting of pyrrole and benzene rings.[24] It has particularly good thermal stability and a slower hydrolytic decomposition rate compared to polyaniline and polypyrrole.[24] PIn has been exploited on sensor, electrocatalysis, anticorrosion, energy storage, supercapacitor, and photocatalysis applications.[24] It can also be used in water purification applications as an adsorbent due to the presence of chelating functional groups in its structure.[23] PIn-ZnO/MgO nanocomposites were used to remove the heavy metals from effluents.[25]

In this study, tBN surface was functionalized with PIn by a simple in situ polymerization process. To the best of our knowledge, this kind of BN composite has not been reported previously. The prepared composite was used for adsorption of U (VI) from liquid phase. The parameters effecting the adsorption capacity were optimized. tBN/PIn exhibited high uptake in low uranium concentrations and low adsorbent amounts. The kinetics and thermodynamic parameters related to adsorption process were determined. A possible adsorption mechanism was suggested using XPS and zeta potential measurements.

2 | MATERIALS AND METHODS

2.1 | Materials

Urea (99%) and B_2O_3 (99.5%) were purchased from Tekim, and Carlo Erba, respectively. Indole monomer (In) (≥99%) and $UO_2(CH_3COO)_2\ 2H_2O$ (uranyl acetate) were supplied from TCI and Merck Co. (Germany), respectively.

2.2 | Methods

2.2.1 | Preparation of tBN

tBN was produced according to the literature[26]: 2 g of boron oxide and 4 g of urea were mixed and finely grounded in a mortar. Then, this powder mixture was heated in an oven at 220°C for 2 h. The precursor material was further heated at 900°C for 2 h in an alumina crucible. The crude product was treated with 10% HCl and washed with ethanol, then dried at 100°C.

2.2.2 | Preparation of PIn and tBN/PIn composite

tBN/PIn was prepared by a facile chemical oxidation reaction of indole/tBN dispersion.[20] For this, tBN (320 mg/100 mL distilled water [DW]) dispersion and In (80 mg/20 mL methanol) solution were ultrasonically mixed for 20 min and then combined. This reaction mixture was cooled to below 5°C. An aqueous solution of ammonium persulfate (200 mg/1 mL DW) was mixed at once with the dispersoid prepared above and stirred for

10974628, 0, Downloaded from https://onlinelibrary.wiley.com/doi/10.1002/app.54856 by Ali Bilici - Canakkale Onsekiz Mart Uni , Wiley Online Library on [09/11/2023]. See the Terms and Conditions (https://onlinelibrary.wiley.com/terms-and-conditions) on Wiley Online Library for rules of use; OA articles are governed by the applicable Creative Commons License

further 6 h. After centrifugation, it was washed four times with water and methanol. The synthesis of PIn was carried out under the same conditions without the use of tBN.

2.2.3 | Adsorption experiments

The batch method was used in the adsorption experiments. The effects of contact times (2–90 min), pH (2.0–8.0), solution concentrations (4–40 mg L^{-1}), and temperatures (297–336 K) on the adsorption were investigated. pH was adjusted with CH_3COOH and NaOH solutions. In the experiments, 0.005 g adsorbent and diluted uranyl acetate solutions (prepared from 100 mg L^{-1} stock) were used. The arsenazo-III complex method was used to determine the final U (VI) concentration after adsorption. In a flask, 1 mL of U (VI) solution was mixed with chloroacetic acid/sodium acetate buffer solution and arsenazo-III reagent, then diluted with 25 mL DW. Absorbance at 650 nm was recorded.[27,28]

The adsorbed U (VI) amount at equilibrium was determined with the Equation (1).

$$q_e = \frac{(C_0 - C_e)}{m} V \quad (1)$$

In the Equation (1) q_e is the adsorbed uranyl amount (mg g^{-1}) at equilibrium, C_0 and C_e were the uranyl ion concentrations (mg L^{-1}) for initial and equilibrium, respectively. V is initial solution volume (L), and m is the adsorbent mass (g).

2.2.4 | Point of zero charge (pH_{PZC}) determination

pH_{pzc} values were determined using drift method.[29,30] 0.005 g adsorbent was added to 0.01 M NaCl (pH 2–10). After mixing for 24 h, final pH was taken, and it was plotted versus the initial pH value.

2.2.5 | Zeta potential determination

Zeta potential measurements of tBN/PIn were conducted before and after adsorption. Before adsorption, 0.005 g adsorbent samples were prepared in 20 mL of DW at different pHs (pH: 3.0–7.0). The zeta potentials of these solutions were measured. For post-adsorption measurements, U (VI) solutions were prepared at the optimum adsorption conditions and different pH values by adding 0.005 g of adsorbent and then the measurements were conducted.

2.2.6 | Selectivity experiments

To determine the adsorbent selectivity, batch experiments were also performed in presence of K^+, Ca^{2+}, Mg^{2+}, Fe^{3+}, and Mn^{2+} solutions. For this, 0.005 g adsorbent was added to 10 mL of aqueous solution of U (VI) and other ions (metal concentration $C_0 = 18$ mg L^{-1}, pH 5.5, $t = 10$ min, $T = 307$ K). After adsorption equilibrium, the concentration of residue ions in the solution was measured by atomic absorption spectroscopy (AAS). The concentration of U (VI) was determined using a spectrophotometric method.

2.2.7 | Characterization techniques

Characterization of the materials was performed via Fourier transform infrared (with a Perkin Elmer Spectrum 100), Raman (using a Witec Alpha 300RA), and UV–Vis (a PerkinElmer Win Lab-25) spectrometers. XRD tests were conducted using a diffractometer (Bruker AXS). TEM analyses were carried out with a Tecnai G2 Spirit Biotwin instrument. Each sample were dispersed in 2 cm^3 methanol, ultrasonically and several drops were added on copper grid and dried before the analyses. A Zeiss Sigma 300 instrument was used for scanning electron microscope analyses (SEM). Before the tests, samples were dispersed in methanol (about 1 mg sample/1.5 mL solvent). Micrometrics 3 Flex model instrument was used for Brunauer–Emmett–Teller (BET) measurements. The degassing was done at 200°C for 5 h. WTW model pH meter (Series 720, Germany) and UV–Vis spectrophotometer (Mecasys, Optizen POP, Korea) were used in adsorption studies. XPS analyses were conducted using Thermo Scientific K-Alpha model instrument equipped with Monochromatic, Al Kα ray source. The acquired XPS spectra was analyzed using a Casa-XPS software. A Malvern Zetasizer Nano ZSP was used for determination of zeta potential of samples before and after adsorption. The concentration of metal ions after adsorption was determined using AAS (Thermo Scientific, ICE-3000 series).

3 | RESULTS AND DISCUSSION

3.1 | Synthesis and characterization of tBN, PIn, and tBN/PIn

tBN/PIn composite was synthesized by O'Connor and oxidative polymerization methods.[26] Urea and B_2O_3 were used as precursor materials to produce tBN. A white colored residue was acquired by calcining the precursors at 900°C for 2 h. tBN/PIn was prepared by chemical

10974628, 0, Downloaded from https://onlinelibrary.wiley.com/doi/10.1002/app.54856 by Ali Bilici - Canakkale Onsekiz Mart Uni , Wiley Online Library on [09/11/2023]. See the Terms and Conditions (https://onlinelibrary.wiley.com/terms-and-conditions) on Wiley Online Library for rules of use; OA articles are governed by the applicable Creative Commons License

oxidative polymerization of tBN-indole dispersion in the presence of APS. The brown colored product was precipitated. Figure 1 schematically illustrates the functionalization of tBN with PIn.

3.1.1 | UV–Vis analysis

The formations of PIn, tBN and tBN/PIn were confirmed by UV–Vis analysis (Figure S1) and matched well with literature reports.[31–33] PIn displayed an absorption peak at 272 nm, which was assigned to π–π* transition.[31] tBN was characterized by absorption maxima at 206 nm, and an absorption tail extending up to 800 nm.[32] For tBN/PIn, the absorptions at 214, 272, and 286 nm were observed. The absorption maxima shifted slightly to higher wavelengths after composite formation as a result of interfacial interaction between the PIn and tBN components.[33]

3.1.2 | FT-IR analysis

FT-IR spectra of tBN, PIn, and tBN/PIn hybrid were given in Figure 2.

tBN exhibited two characteristic peaks at 1336 cm^{-1} (B-N stretching vibrations), and 754 cm^{-1} (B-N-B bending vibrations).[34] IR spectrum of PIn exhibited following

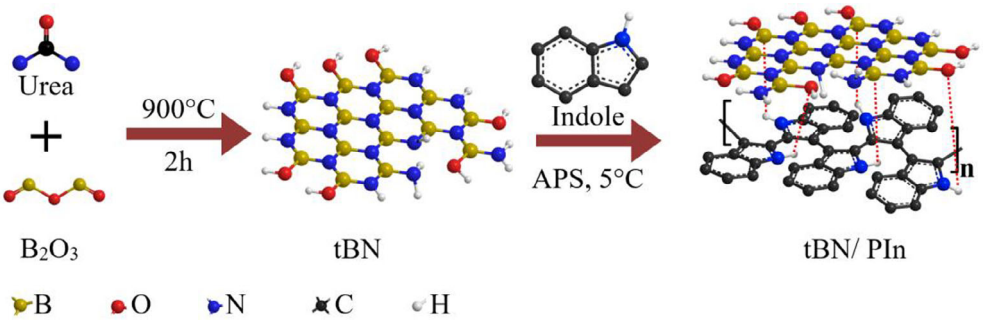


FIGURE 1 The synthesis scheme of tBN, and tBN/PIn. [Color figure can be viewed at wileyonlinelibrary.com]

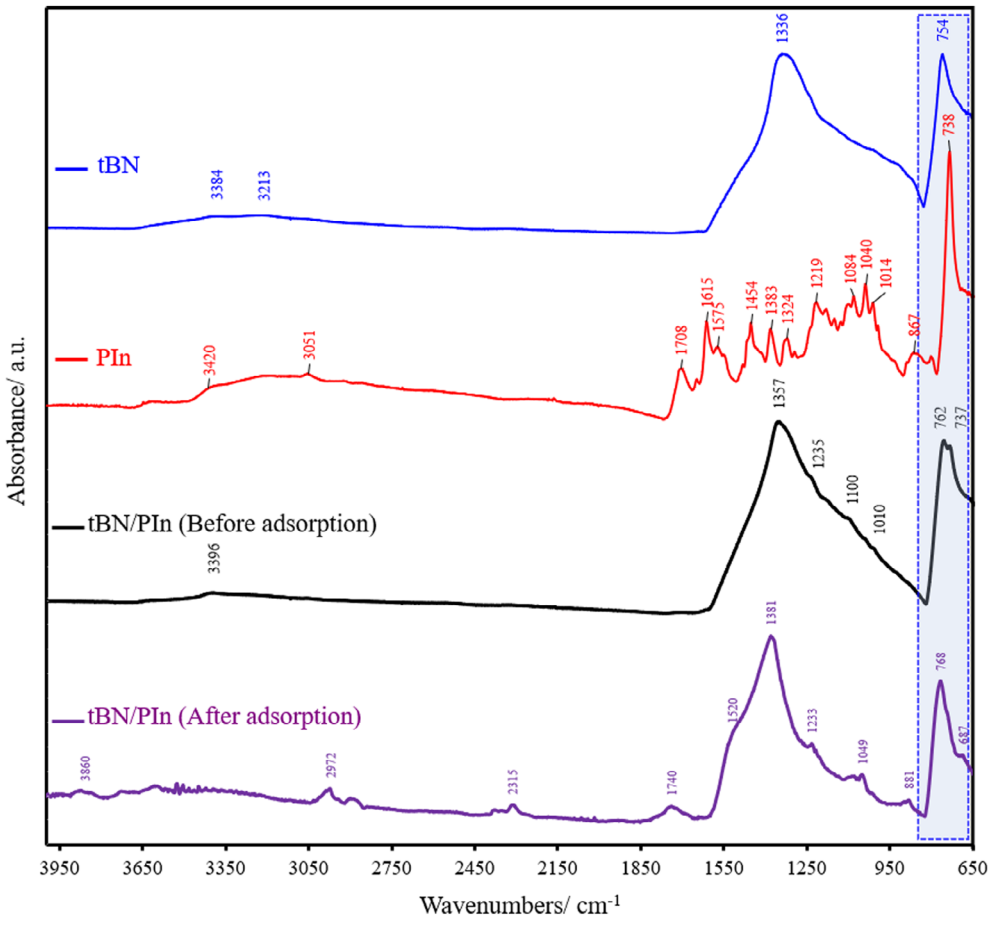


FIGURE 2 FT-IR spectra of tBN, PIn, and tBN/PIn. [Color figure can be viewed at wileyonlinelibrary.com]

10974628, 0, Downloaded from https://onlinelibrary.wiley.com/doi/10.1002/app.54856 by Ali Bilici - Canakkale Onsekiz Mart Uni , Wiley Online Library on [09/11/2023]. See the Terms and Conditions (https://onlinelibrary.wiley.com/terms-and-conditions) on Wiley Online Library for rules of use; OA articles are governed by the applicable Creative Commons License

main peaks: 3420, 3051, 1708, 1615, 1575, 1454, 1383, 1084, 1040, and 738 cm^{-1}. The peaks at 3420, 1615, and 738 cm^{-1} were observed due to N–H stretching, N–H and benzene ring deformations, respectively.[35] The peaks at 1454 and 1575 cm^{-1} belong to the stretching vibrations of C–C bonds in PIn benzene rings.[36] The peak at 1383 cm^{-1} corresponded to the C–N vibration bonds. The peak around at 1708 cm^{-1} was assigned to carbonyl stretching vibrations of pyrrole ring (N–C=O).[35] The absorption intensities and positions of the bands of tBN were changed after oxidation process due to the interaction between PIn and tBN matrix. B-N stretching (1336 cm^{-1}) and B-N-B (754 cm^{-1}) bending vibrations shifted to 1357, and 762 cm^{-1}, respectively. These shifts in the FT-IR absorption peaks was probably the result of secondary interactions between PIn and tBN.[34] These similar spectral findings were also reported for composite of BN with polypyrrole.[20]

3.1.3 | Raman analysis

Figure S2 belongs to Raman spectra of the tBN, PIn and tBN/PIn. The major scattering peak at 1373 cm^{-1} was characteristic vibrational mode for tBN.[37,38] For PIn, the broad peaks centered at 1335 cm^{-1} (C−N stretching vibrations), and 1565 cm^{-1} (C=N stretching vibrations) were noticed. tBN/PIn exhibited a major peak at 1356 cm^{-1} belong to BN component, and minor and weaker peaks at 1544 and 1613 cm^{-1} belong to PIn component, respectively. It was noted that major scattering peak of tBN shifted to 1356 cm^{-1} after polymerization process because of interaction between tBN and PIn constituents. These results verified the successful indole polymerization on the tBN surface.

3.1.4 | XRD analysis

XRD pattern of tBN, PIn and tBN/PIn hybrid are represented in Figure 3.

XRD pattern of PIn revealed three broad peaks at 2θ value of 8.3, 19.8, and 26.6°. The presence of broad diffraction peaks confirmed the formation of an amorphous polymer structure.[39] The diffraction peak observed at 2θ value of 8.3° was attributed to the distance between nitrogen atoms and dopant molecules.[40] tBN were characterized with two main diffraction peaks: the sharp diffraction peak at 2θ value between 23 and 29° (centered at 27.0°) and the broad peak at 40–45° (centered at 42.3°) were in harmony with the Bragg angles of (002) and (10×) reflections (inseparable 100 and 101 peaks of BN), respectively. These data proved the formation of tBN structure.[41,42] After the surface modification of tBN with

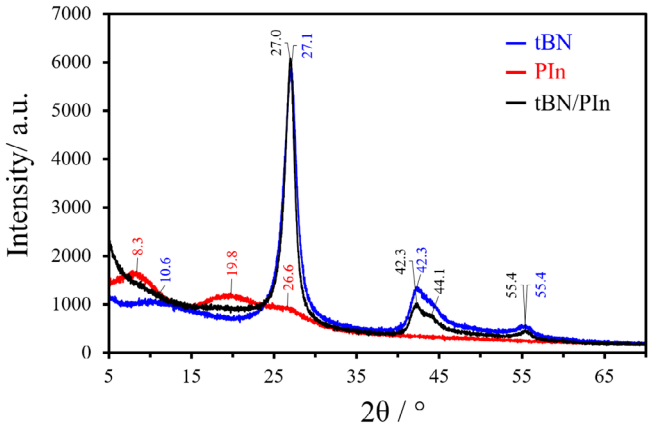


FIGURE 3 XRD spectra of tBN, PIn, and tBN/PIn. [Color figure can be viewed at wileyonlinelibrary.com]

PIn, a slight shift in the peak position at $2\theta = 27.0°$ was observed. In addition, a slight attenuation of (10×) plane peak intensity (centered 42.3°) was realized. This assigned tBN surface was functionalized successfully with PIn. The diffraction spectrum of the composite did not exhibit any characteristic peaks for PIn. This may be attributed to its amorphous structure or low amount on the tBN surface.[43]

3.1.5 | TEM and SEM analysis

Morphological analysis of tBN, PIn and tBN/PIn were studied by TEM and SEM techniques. Figure 4 belong to TEM images of the samples.

As seen in Figure 4a, b, tBN were composed of agglomerated nanoparticles. Particle population was almost homogeneous, and the nanoparticle size ranged from 7 to 10 nm. It was interesting that PIn also exhibited a similar morphology (Figure 4c, d). The particle sizes changed between 7 and 10 nm. These images were consistent with the morphology of indole polymers previously reported.[44] However, as seen in Figure 4e, f, hybrid structure exhibited a web-like more ordered morphology. This assigned that PIn was dispersed on the tBN matrix during the in-situ polymerization. tBN-polyaniline composite was also presented a similar morphology.[45]

Figure 5a–d shows the SEM images of samples before adsorption.

SEM images of tBN (Figure 5a) showed the presence of tightly packed, unshaped nanoparticles having different dimensions. However, template-free synthesis of PIn presented well defined microspheres (Figure 5b). The similar SEM images were reported before for $FeCl_3$[46] and APS[40] triggered synthesis of polyindole. SEM images of the composite before and after adsorption were presented in Figure 5c–f, respectively. After the oxidation process,

10974628, 0, Downloaded from https://onlinelibrary.wiley.com/doi/10.1002/app.54856 by Ali Bilici - Canakkale Onsekiz Mart Uni , Wiley Online Library on [09/11/2023]. See the Terms and Conditions (https://onlinelibrary.wiley.com/terms-and-conditions) on Wiley Online Library for rules of use; OA articles are governed by the applicable Creative Commons License

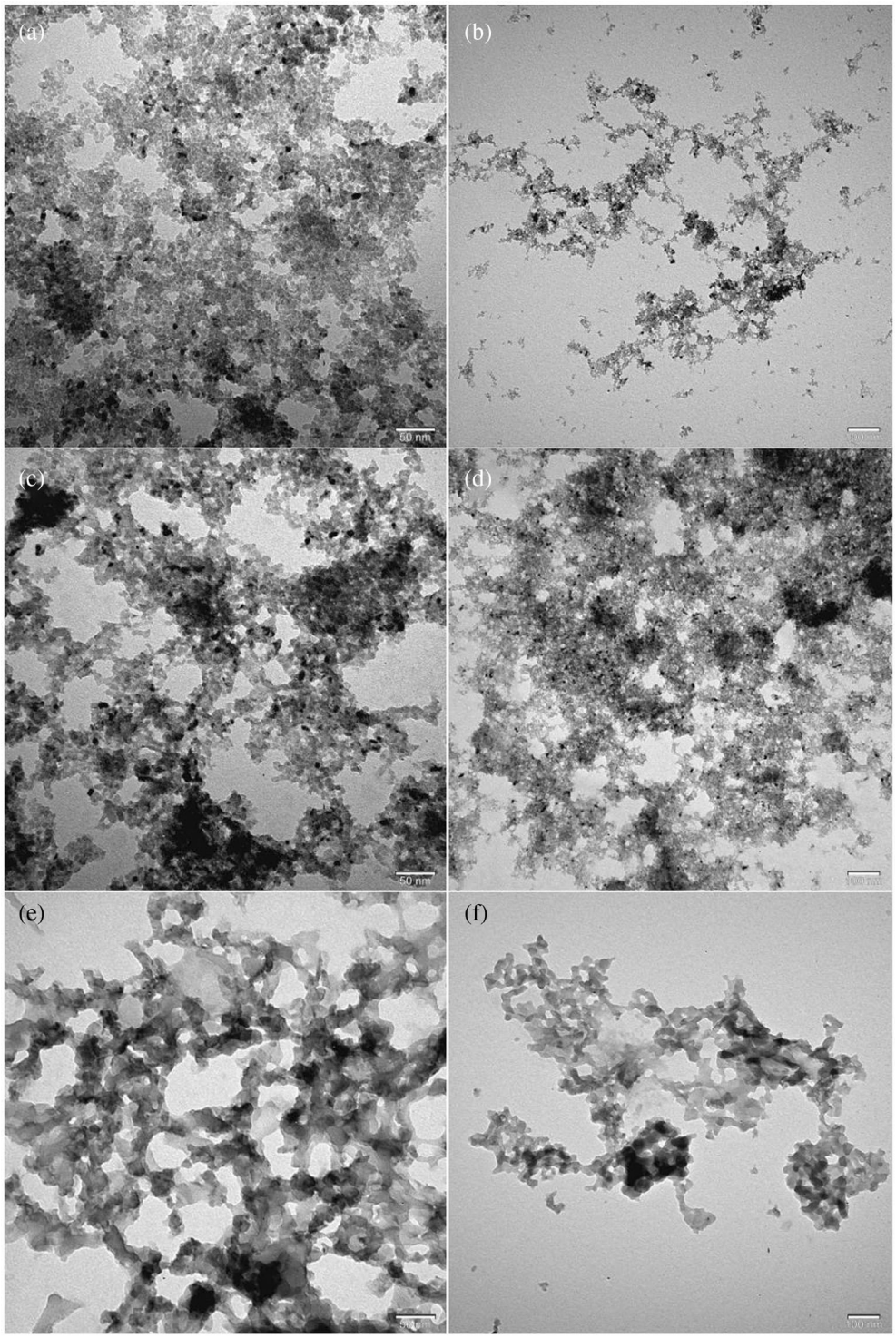


FIGURE 4 TEM images of tBN (a, b), PIn (c, d), and tBN/PIn. (e, f) (Bar shows 50 nm in the left column, and 100 μm in the right column).

original tBN morphology was changed. As seen in Figure 5c, d, tBN/PIn had sub-micron sized, heterogeneous and tightly packed particles. Due to the difficulty of determining the presence of PIn on the tBN matrix by SEM and TEM analysis alone, EDX elemental analysis and elemental mapping techniques were used (Figures S3 and S4).[34] C, N, O, and S elemental ratios of PIn revealed by EDX analysis (as mean weight %) were 72.22, 8.63, 7.88, and 11.27, respectively. B, O and N ratios for tBN were found to be 35.65, 45.38, and 18.97, respectively. As for tBN/PIn (after adsorption process), B, C, N, and O elemental ratios were 22.84, 17.02, 46.29, and 13.34, respectively. The presence of C atoms (Figure S3c) showed the successful coating of tBN surface with PIn. In addition, high N content of the hybrid (46.29% as mean weight) may be an indication of the alkaline nature of adsorbent surface. The distribution of elements on the t-BN matrix was monitored by elemental mapping technique

10974628, 0, Downloaded from https://onlinelibrary.wiley.com/doi/10.1002/app.54856 by Ali Bilici - Canakkale Onsekiz Mart Uni , Wiley Online Library on [09/11/2023]. See the Terms and Conditions (https://onlinelibrary.wiley.com/terms-and-conditions) on Wiley Online Library for rules of use; OA articles are governed by the applicable Creative Commons License

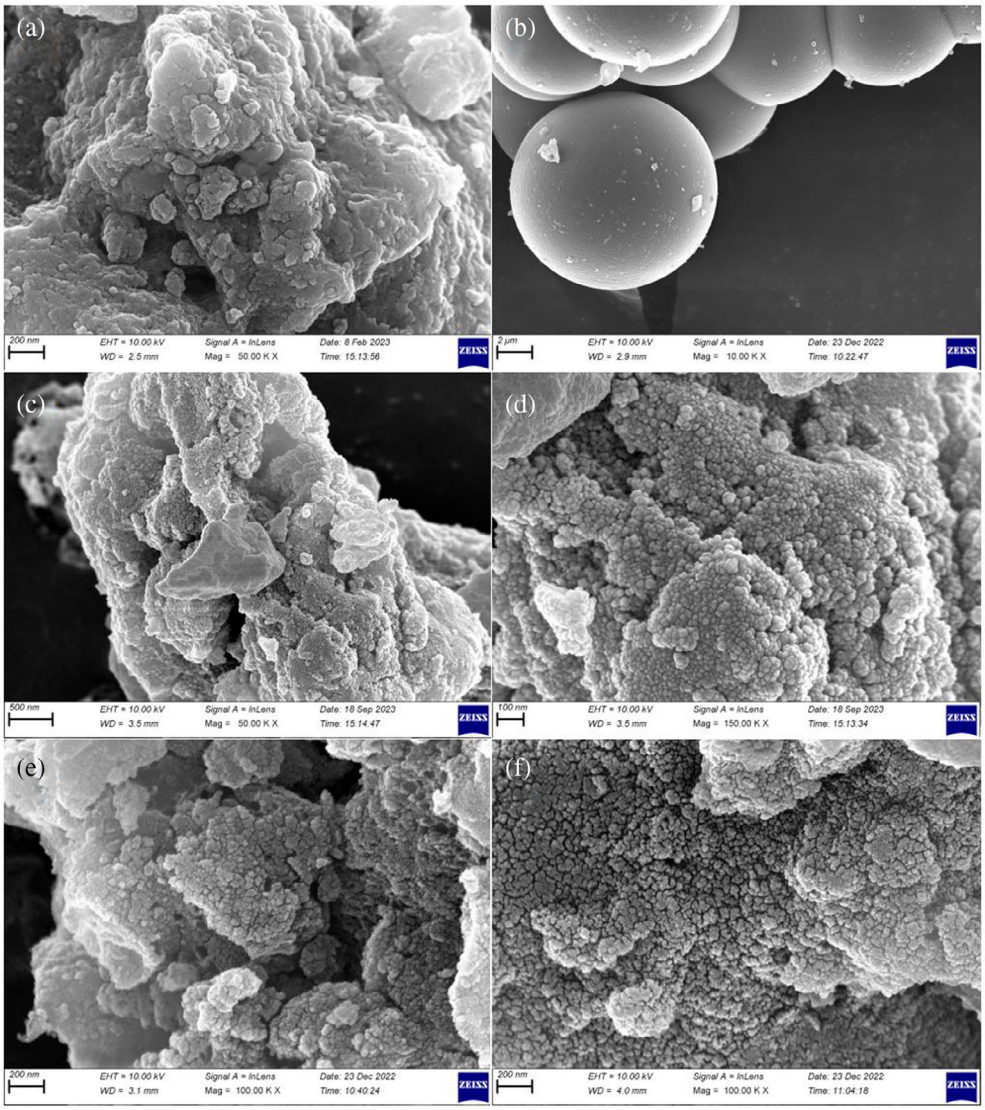


FIGURE 5 SEM images of tBN (a), PIn (b), and tBN/PIn before (c, d) and after (e, f) adsorption. [Color figure can be viewed at wileyonlinelibrary.com]

(Figure S4). As seen in Figure S4, carbon, and nitrogen elements were uniformly distributed on tBN surface. This indicates the almost homogeneous PIn distribution on the tBN.

3.1.6 | XPS analysis

Elemental composition and functional groups of the tBN/PIn were investigated by XPS analysis (Figure S5). As seen from XPS full spectrum, N1s, B1s, C1s, and O1s signals of the tBN/PIn were located at 398.58, 190.88, 284.63, and 532.80 eV, respectively (Figure S5a). B1s spectra given in Figure S5b exhibited a B-N peak at 190.69 eV, and a B-O peak at around 191.86 eV. B-O peak may result from the hydroxylation of BN surface.[47] Three peaks at 284.34, 284.98, and 285.18 eV were observed in C1s spectrum of sample, corresponding to aromatic C=C, C−C, and C−N bonds, respectively (Figure S5c).[35] In the N1 spectra, three peaks were observed at 398.05, 398.78, and 400.71 eV, corresponding to the B–N, C–N, and –NH_2 bonds, respectively (Figure S5d).[47] O1s spectra displayed a peak at 532.79 eV due to the hydroxyl groups in the composite structure (Figure S5e).[47] Atomic ratios of N, B, C, and O were found to be 31.61%, 37.84%, 22.27%, and 8.28%, respectively (Figure S5a). The atomic ratio of the C in the tBN/PIn nanocomposite (22.27%) were close to the experimental amount of PIn added to composite (20%), which confirmed the successful synthesis of the tBN/PIn.

3.1.7 | BET analysis

The total pore volumes, average pore diameters, and specific surface areas of PIn, tBN, and tBN/PIn were determined by multi-point BET analysis and Barrett–Joyner–Halenda (BJH) adsorption–desorption method and were given in Table S1. N_2 adsorption–desorption isotherms of the adsorbent (Figure S6) were observed to be in

10974628, 0, Downloaded from https://onlinelibrary.wiley.com/doi/10.1002/app.54856 by Ali Bilici - Canakkale Onsekiz Mart Uni , Wiley Online Library on [09/11/2023]. See the Terms and Conditions (https://onlinelibrary.wiley.com/terms-and-conditions) on Wiley Online Library for rules of use; OA articles are governed by the applicable Creative Commons License

harmony with the type IVa physisorption isotherm typically given by porous adsorbents in the IUPAC classification, and it was assumed that the initial monolayer-multilayer adsorption on the mesopore walls was followed by pore condensation.[48] Furthermore, the adsorption–desorption isotherm resembled the H4 loop, one of the hysteresis loops defined by IUPAC, which associated with the filling of reversible micropores at low p/p_0 followed by multilayer physical adsorption and capillary condensation. The activated carbons and some other nanoporous adsorbents exhibited similar loop.[48,49] According to BET analysis data, a decrease was observed in the surface area of the hybrid material compared to tBN. On the contrary, there was an increase in total pore volume and average pore diameter. Average pore diameters of PIn, tBN, and tBN/PIn were 32.522, 20.06, and 49.815 Å, respectively. The same proportional changes were also presented in the data obtained from the BJH method. This presumably caused by the reduction of the pore wall thicknesses and the destruction of the walls of the hybrid structure.[49–51]

3.2 | Adsorption applications

The adsorption tests were carried out to determine the effects of pH, initial U (VI) concentration, adsorption time and temperature on the adsorbent. In these experiments, stirring speed was 720 rpm, and adsorbent amount was 0.005 g/10 mL.

3.2.1 | pH effect

In order to determine the effect of pH on adsorption, the studies were performed at pH values in the range of 3.0–8.0, at U (VI) concentration of 10 mg L^{-1} for 1 h contact time. The highest of adsorbed U (VI) amount at equilibrium (q_e) was obtained in the pH range of 5.0–5.5 (Figure S7). The changes in pH could affect both the surface charge and binding sites of the adsorbent.[48] Therefore, zeta potentials of tBN/PIn were measured before and after adsorption and plotted versus pH (Figure S8). As seen in Figure S8, the surface of the adsorbent became positively charged before adsorption due to the surface protonation at low pH values and became negatively charged as the pH increased. However, after adsorption, tBN/PIn surface were negatively charged at all pH values studied. The negative zeta potential at all pH values after adsorption indicated that the adsorbent surface was coated with U (VI) ions and that the adsorption process led to the formation of negatively charged groups on the adsorbent surfaces.[52] Hence, the zeta potential values of tBN/PIn became less negative as pH of the aqueous solution decreased, possibly due to the protonation of tBN/PIn functional groups (hydroxyl and amino groups). In low pH values (2.0–5.0), U (VI) cationic species such as UO_2^{2+}, UO_2OH^+, and $(UO_2)_3(OH)_5^+$ were available in the solution.[53] A competitive adsorption between H_3O^+ ions and U (VI) cationic species were formed in the solution, and this leads to electrostatic repulsion between them. This results to a decrease in the adsorption.[54] The increase in pH from 5.0 to 5.5 resulted in the formation of negatively charged U (VI) species, which enhanced the electrostatic attraction, thus increasing the adsorption.[9,48,55,56] Above pH 5.5, anionic species of U (VI) complexes such as $(UO_2)_3(OH)^{7-}$, $UO_2(OH)^{3-}$, and $UO_2(OH)_4^{2-}$ were formed and this leads to a significant decrease in adsorption.[53,57]

As seen in the pH_{PZC} graph (Figure S9), at low pH values, adsorbent surface was positively charged, while it was negatively charged as pH values increased. The protons and cations in the solution are more adsorbed on surface at low pH, while as the pH rises, deprotonation on the adsorbent surface begins and the retention of hydroxyl ions on the surface increases.

3.2.2 | Contact time effect and adsorption kinetics

The effects of contact time between 2 and 90 min were investigated as other parameters constant. The adsorption equilibrium was established in the 10th minute and the highest adsorption efficiency was obtained in this period (Figure 6a). The initial stage of adsorption (up to 10th minute) was rapid likely due to the abundance of reaction sites on the adsorbent surface. However, the decrease in adsorption efficiency after reaching equilibrium (after 10th minute) may be attributed a gradually decrease in these sites and saturated by U (VI) ions.

To determine the U (VI) adsorption kinetics, different kinetic models (pseudo first-order [PFO],[58–60] pseudo-second-order [PSO], and intra-particle diffusion [IPD]), were applied to the data obtained from the experiments for various contact times. Related Equations (2)–(4) are given below.

$$\ln(q_e - q_t) = \ln q_e - k_1 t \tag{2}$$

$$\frac{t}{q_t} = \frac{1}{k_2 {q_e}^2} + \frac{1}{q_e} t \tag{3}$$

$$q_t = K_{id} t^{1/2} + I \tag{4}$$

In Equations (2)–(4) q_t and q_e are the amount of adsorbed radionuclide for a t time and equilibrium,

10974628, 0, Downloaded from https://onlinelibrary.wiley.com/doi/10.1002/app.54856 by Ali Bilici - Canakkale Onsekiz Mart Uni , Wiley Online Library on [09/11/2023]. See the Terms and Conditions (https://onlinelibrary.wiley.com/terms-and-conditions) on Wiley Online Library for rules of use; OA articles are governed by the applicable Creative Commons License

respectively (mg g^{-1})·k_1 (min^{-1}), k_2 (g mg^{-1} min^{-1}), and K_{id} (mg g^{-1} $min^{-1/2}$) are the PFO, PSO, and IPD rate constants, respectively.

Kinetic parameters calculated using Equations (2)–(4) were given in Table 1. These data indicated that the U (VI) adsorption kinetics fitted for the PSO kinetic model (Figure 6). Additionally, the graph drawn using the non-linear equations of the kinetic models is shown in Figure S10.

The PSO kinetic model is suitable to describe the adsorption phenomenon at low concentrations.[61] Azizian (2004) also reported that the adsorption kinetics could be clarified better by PSO kinetics when the solution concentration (C_0) was low.[62] However, the adsorption fitted for PFO kinetics as the C_0 values increased. In addition, the line drawn in the IPD model did not intersect the origin. This indicated the adsorption process took place in a short time.[63]

3.2.3 | Initial concentration effect and equilibrium of adsorption

The initial U (VI) concentration was another parameter affecting the adsorption. The experiments were conducted in the adsorbent concentration of 4–40 mg L^{-1} while keeping the other parameters constant (contact time: 10 min, uranyl concentration: 10 mg L^{-1}, temperature: 25°C, adsorbent amount: 0.005 g). As initial ion concentration (4 mg L^{-1}) increased up to 18 mg L^{-1}, an adsorption equilibrium was established, and the maximum adsorption was observed.

Data obtained from these experiments were applied to four different isotherm models (Freundlich, Langmuir, Redlich-Peterson, and Dubinin-Radushkevich) to elucidate the adsorption equilibrium.[64–67] The non-linear equations of the isotherms and the calculated isotherm parameters were demonstrated in Table S2, and the plots drawn for these isotherms given in Figure 7.

Non-linear adsorption isotherms were applied to define the adsorption equilibrium. As seen that the adsorption equilibrium was compatible with both Langmuir and Freundlich, and Redlich-Peterson (RP) isotherms ($R^2 = 0.994$ in three isotherms). This data ($R^2 = 0.994$) indicated that U(VI) adsorption on tBN/PIn was monolayer. As the β value in the RP equation approached 1, the isotherm resembled the Langmuir equation. As the K value is big enough, the isotherm resembles the Freundlich equation.[68] R_L value calculated using the Langmuir constant (b) was between 0 and 1 ($R_L = 0.575$). This indicated that adsorption process was appropriate. Freundlich constant n takes a value

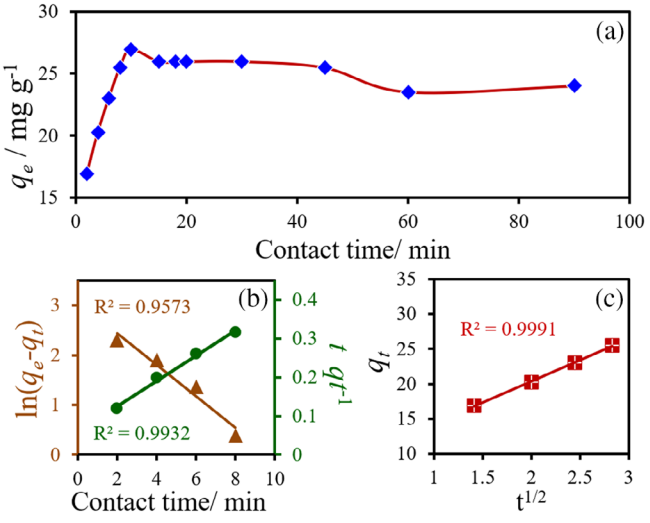


FIGURE 6 The time dependent amount of adsorbed U (VI) ions (a), PFO (-▲- in b), PSO (-●- in b), and IPD (c) kinetic plots of U (VI) adsorption on tBN/PIn at $C_0 = 10$ mg L^{-1}, pH = 5.0–5.5, 25°C, $m/V = 0.005$ g adsorbent/10 mL solution. [Color figure can be viewed at wileyonlinelibrary.com]

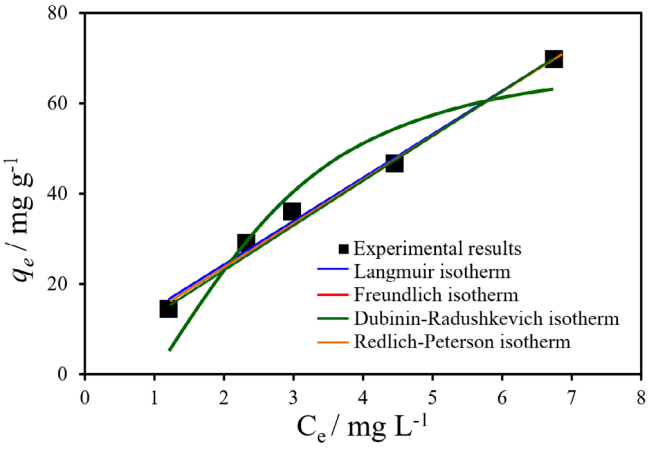


FIGURE 7 Influence of solution concentration on the U (VI) adsorption and related non-linear isotherm plots. [Color figure can be viewed at wileyonlinelibrary.com]

TABLE 1 The kinetic parameters of U(VI) adsorption onto tBN/PIn.

Pseudo-first-order			Pseudo-second-order			Intra-particle diffusion		
k_1 (min^{-1})	q_{e1} (mg g^{-1})	R^2	k_2 (g mg^{-1} min^{-1})	q_{e2} (mg g^{-1})	R^2	K_{id} (mg g^{-1} $min^{-1/2}$)	I	R^2
0.315	21.46	0.957	0.018	30.488	0.993	6.062	8.232	0.999
Experimental value			q_{exp} (mg g^{-1})		26.95			

10974628, 0, Downloaded from https://onlinelibrary.wiley.com/doi/10.1002/app.54856 by Ali Bilici - Canakkale Onsekiz Mart Uni , Wiley Online Library on [09/11/2023]. See the Terms and Conditions (https://onlinelibrary.wiley.com/terms-and-conditions) on Wiley Online Library for rules of use; OA articles are governed by the applicable Creative Commons License

between 1 and 10 ($n = 1.167$). This also indicated the formation of the adsorption process between uranyl ions and tBN/PIn.[69,70] However, the heterogeneity factor, $1/n$, which was calculated from the Freundlich constant (n) and expressed the surface heterogeneity between the adsorbent and the adsorbate, was found to be 0.856. More heterogeneity of the surface is expressed by the $1/n$ being close to 0.[71] The average energy value of adsorption (E) obtained from the Dubinin-Radushkevich equation gives information about the nature of the adsorbent-adsorbate interaction ($E < 8$ kJ mol^{-1}: physical forces, $8 < E < 16$ kJ mol^{-1}: ion exchange, $E > 16$ kJ mol^{-1}: chemical sorption).[72] E value was found to be 0.658 kJ mol^{-1} implied that the adsorption process was controlled by weak Van der Waals interactions and physical forces, such as physical sorption.

The maximum adsorption capacity (q_m) was 315.29 mg g^{-1} as given above. The allowed uranium level in drinking water is 30 μg L^{-1}.[2,73] Therefore, it is important to develop innovative adsorbents, which eliminate exceptionally low uranium concentrations from liquid phase. Even if the amount of uranium remaining after absorption is very low, this is a significant risk to health. It was noted that the uranium levels remaining after adsorption in this study were too low to pose a health threat. Our results were compared with those of recently published studies (Table 2). For a simple comparison, the adsorption efficiency of tBN was also studied in the conditions of pH = 5.0–5.5, $T = 307$ K, $t = 10$ min, $C_0 = 18$ mg L^{-1} (optimum conditions for tBN/PIn). tBN removed the 66.88% of the U (VI) from aqueous solution, while tBN/PIn removed 98.91% at same conditions.

3.2.4 | Temperature effect and adsorption thermodynamics

The experiments were also performed in the range of 283–338 K to determine the temperature effect on the adsorption process. It was found that adsorption was endothermic at low temperatures (283–298 K), and exothermic at high temperatures (307–338 K) (Figure S11a). The standard enthalpy (ΔH°) and entropy (ΔS°) changes were obtained from the graph (ln K_{eq} vs. $1/T$) drawn using the Van't Hoff Equation (5), and the Gibbs free energy change (ΔG°) values at each temperature were found from the Equation (6).[79,80]

$$\ln K_{eq} = -\frac{\Delta H^\circ}{RT} + \frac{\Delta S^\circ}{R} \quad (5)$$

$$\Delta G^\circ = \Delta H^\circ - T\Delta S^\circ \quad (6)$$

In Equations (5) and (6), K_{eq}, R, and T correspond to the coefficient for thermodynamic distribution, the gas constant (8.314 J mol^{-1} K^{-1}), and temperature (K), respectively.

Thermodynamic parameters for different temperature ranges, calculated from the graph given in Figure S11b, are presented in Table 3.

TABLE 2 Comparison of U(VI) removal efficiency of various composite adsorbents.

Adsorbent	C_0 (mg L^{-1})	Adsorbent dosage (g)	Adsorption capacity (mg g^{-1})	References
Ap-ZnO/PSBN nanocomposite	70–800	0.10	139.80	74
Poly(vinyl alcohol)/carbon nanotube composites	100–1000	0.03	232.55	75
Hydroxyapatite/white clay nanocomposite	119	0.05	570–670	76
MXene/graphene oxide nanocomposites	100	0.10	1003.50	77
Magnetically modified hydroxyapatite	150–300	0.025–0.09	310	78
tBN/PIn	2–40	0.005	315.29	This study

TABLE 3 Thermodynamic parameters for U (VI) adsorption.

Temperature range	ΔH° (kJ mol^{-1})	ΔS° (kJ/mol^{-1} K^{-1})	ΔG° (kJ mol^{-1})			
283–298 K	81.88	0.31	283	288	293	298
			−5.01	−6.54	−8.07	−9.61
307–338 K	−47.36	−0.12	307	316	326	336
			−11.44	−10.39	−9.22	−8.05

10974628, 0, Downloaded from https://onlinelibrary.wiley.com/doi/10.1002/app.54856 by Ali Bilici - Canakkale Onsekiz Mart Uni , Wiley Online Library on [09/11/2023]. See the Terms and Conditions (https://onlinelibrary.wiley.com/terms-and-conditions) on Wiley Online Library for rules of use; OA articles are governed by the applicable Creative Commons License

A positive adsorption enthalpy value (ΔH°) at low temperatures indicated that the U (VI) adsorption onto tBN/PIn was endothermic, while at elevated temperatures, adsorption decreases, and the adsorption became exothermic. The adsorption entropy value (ΔS°) was positive at low temperatures, indicating that adsorption tended to be spontaneous. The adsorption at low temperatures had lower Gibbs free energy values (ΔG°) as the temperature increased; this was also an indication of the possibility of the adsorption process and supported the tendency of adsorption to be spontaneous.

3.3 | Predicted adsorption mechanism

The adsorption mechanism on the adsorbent surface can be explained by interface interactions such as electrostatic interactions, weak physical adsorption via Van der Waals forces, Lewis acid–base interactions, hydrogen bonds, steric interaction, complex formation, ion exchange and covalent bonding.[81,82] FTIR, SEM, EDX, zeta potential measurements, and XPS analysis were performed to evaluate the changes in composite structure after U (VI) adsorption. Figure 2 shows the FTIR spectra of tBN/PIn surface before and after uranyl adsorption. After adsorption, FTIR absorption peaks of tBN/PIn (1357, and 762 cm^{-1}) were red-shifted. In addition, new absorption bands were observed in range from 2300 to 3860 cm^{-1}, and 880 to 1750 cm^{-1}, which were in harmony with amine and imine stretching vibrations.[3] tBN/PIn contained substantial amount of free amino/imine groups, thus its surface presented alkalinity.[3] SEM images showed that the original surface morphology of tBN/PIn was almost maintained after U(VI) adsorption (Figure 5e, f). SEM–EDX analyses confirmed the high nitrogen content of tBN/PIn after adsorption process, as seen in Figure S3. These groups may coordinate with U(VI) via electrostatic interactions as described before.[83]

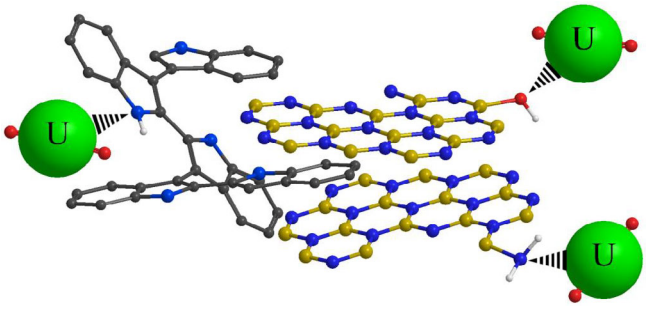


FIGURE 8 Predictive UO_2^{2+} adsorption mechanism onto tBN/PIn surface. [Color figure can be viewed at wileyonlinelibrary.com]

Zeta potential measurements confirmed the existence of this interaction discussed above. To gain further information about the adsorption mechanism, XPS analysis of tBN/PIn were conducted before and after uranium adsorption. After adsorption, the peaks of U $4f^{5/2}$ and U $4f^{7/2}$ were observed around 381.81, and 392.87 eV, respectively. U content was determined to be 0.05%. As compared the O 1 s peaks of tBN/PIn before and after adsorption, the presence of a new O-U peak (531.02 eV) was realized (Figures S5e and S5j).[35] This assigned the U atom was coordinated with O atoms of the adsorbent as shown in Figure 8, and in harmony with the results of Zhang and coworkers.[84] As a result, at first, adsorption mechanism could involve electrostatic interaction in solution between U (VI) ions and oxygen atoms of composite as shown. Following this, a complexation and redox reaction were developed between them as suggested by Lai and coworkers.[53]

3.4 | Selectivity studies

The adsorption batch experiments were also performed in presence of other metal ions (K^+, Ca^{2+}, Mg^{2+}, Mn^{2+}, Fe^{3+}) prepared at equivalent concentrations. Multiple ion mixtures were prepared synthetically considering the composition of nuclear industrial wastewater.[85–87] The percentage of adsorption value determined are presented in Figure 9. As seen in Figure 9, the tBN/PIn was better adsorbent for UO_2^{2+} ions as compared to other metal ions, except for Fe^{3+} ions. It was observed that the affinity of TBN/PIN to other metals changed in the following order: $Fe^{+3} > UO_2^{2+} > Mn^{+2} > Mg^{+2} > K^{+1} > Ca^{+2}$. Fe^{3+} and Mn^{2+} ions, being in the same hard acid group as UO_2^{2+} ions and interfering with each other in

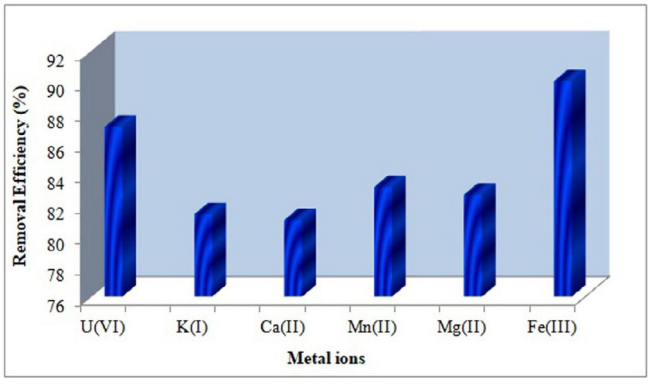


FIGURE 9 Selective adsorption percentages of UO_2^{2+} and other ions by tBN/PIn ($C_0 = 18$ mg L^{-1}, pH 5.5, $t = 10$ min, $m_{adsorbent} = 0.005$ g, $T = 307$ K). [Color figure can be viewed at wileyonlinelibrary.com]

10974628, 0, Downloaded from https://onlinelibrary.wiley.com/doi/10.1002/app.54856 by Ali Bilici - Canakkale Onsekiz Mart Uni , Wiley Online Library on [09/11/2023]. See the Terms and Conditions (https://onlinelibrary.wiley.com/terms-and-conditions) on Wiley Online Library for rules of use; OA articles are governed by the applicable Creative Commons License

the solution. Although Ca^{2+} and Mg^{2+} ions were divalent cations such as UO_2^{2+} ions, they did not reduce the selectivity of the adsorbent for uranium. This competitive adsorption means that UO_2^{2+} ions can be adsorbed on the tBN/PIn composite even in the presence of other metal ions without any significant interference, except for Fe^{3+} ions.

4 | CONCLUSION

A novel tBN composite (tBN/PIn) was prepared, characterized, and used as a potential adsorbent for U (VI) removal from aqueous solution. When tBN was functionalized with PIn, Lewis basic groups increased on its surface. After the hybridization, total pore volume and average pore diameter of tBN/PIn (0.196 $cm^3\ g^{-1}$, 49.815 Å) increased as compared to those of tBN (0.157 $cm^3\ g^{-1}$, 20.06 Å) and PIn (0.0047 $cm^3\ g^{-1}$, 32.522 Å). The optimum uranyl adsorption conditions were determined to be pH = 5.0–5.5, $T = 307$ K, $t = 10$ min, $C_0 = 18$ mg L^{-1}. Freundlich, Langmuir and Redlich-Peterson isotherms were used to explain the adsorption model fitting analysis. From the Langmuir isotherm, the maximum U (VI) adsorption capacity (q_m) of tBN/PIn was determined to be 315.29 mg g^{-1} ($R^2 = 0.994$). U (VI) adsorption kinetics were better explained by PSO kinetic, which was more suitable for describing the adsorption event at low concentrations. Adsorption thermodynamics parameters (ΔG°, ΔH°, and ΔS°) were also determined and it was observed that the adsorption process was endothermic at low temperatures, tended to occur spontaneously, and increased spontaneously as the temperature increased. The development of new types of tBN—conductive polymer composites will contribute to the production of innovative adsorbents with developed functionality and surface properties.

AUTHOR CONTRIBUTIONS

Deniz Emre: Conceptualization (supporting); investigation (equal); visualization (lead); writing – original draft (equal); writing – review and editing (lead). **Özlem Selçuk Zorer:** Conceptualization (lead); formal analysis (lead); investigation (lead); writing – original draft (lead); writing – review and editing (lead). **Ali Bilici:** Conceptualization (lead); funding acquisition (lead); project administration (lead); writing – original draft (lead); writing – review and editing (lead). **Erhan Budak:** Investigation (supporting); writing – review and editing (supporting). **Selehattin Yilmaz:** Supervision (equal); writing – review and editing (supporting). **Necla Caliskan Kilic:** Conceptualization (equal); investigation (equal); writing – original draft (equal); writing – review and editing (supporting). **Eda Gokirmak Sogut:** Visualization (supporting); writing – original draft (supporting).

ACKNOWLEDGMENTS

Çanakkale Onsekiz Mart University Scientific Research Commission supported this work (Grant number FBA-2022-4033).

CONFLICT OF INTEREST STATEMENT

The authors declare no conflicts of interest.

DATA AVAILABILITY STATEMENT

Data will be made available on request.

ORCID

Deniz Emre https://orcid.org/0000-0003-0493-8154
Özlem Selçuk Zorer https://orcid.org/0000-0002-6486-8365
Ali Bilici https://orcid.org/0000-0002-1377-5580
Erhan Budak https://orcid.org/0000-0002-6476-8639
Selehattin Yilmaz https://orcid.org/0000-0003-4607-3523
Necla Caliskan Kilic https://orcid.org/0000-0001-5451-3192
Eda Gokirmak Sogut https://orcid.org/0000-0002-7707-3924

REFERENCES

[1] T. P. Gandhi, P. V. Sampath, S. M. Maliyekkal, *Sci. Total Environ.* **2022**, *825*, 153947.
[2] WHO, Management of radioactivity in drinking-water; Geneva (2018).
[3] L. Li, Y. Zhao, Y. Jin, W. Linghu, C. Chen, A. M. Asiri, H. M. Marwani, G. Sheng, *J. Radioanal. Nucl. Chem.* **2019**, *321*, 1035.
[4] IAEA, *Treatment of liquid effluent from uranium mines and mills*, International Atomic Energy Agency, Vienna **2004**.
[5] A. Mellah, S. Chegrouche, M. Barkat, *Hydrometallurgy* **2007**, *85*, 163.
[6] I. Ihsanullah, *Chemosphere* **2021**, *263*, 127970.
[7] J. Yang, B. Volesky, *Water Res.* **1999**, *33*, 3357.
[8] A. C. Q. Ladeira, C. A. Morais, *Miner. Eng.* **2005**, *18*, 1337.
[9] C. Wang, D. Huang, F. He, T. Jin, B. Huang, J. Xu, Y. Qian, *ACS Omega* **2020**, *5*, 27789.
[10] A. Chakraborty, A. Pal, B. B. Saha, *Materials* **2022**, *15*, 8818.
[11] M. Öztürk, Ö. S. Zorer, M. Gülcan, *Colloids Surf. A Physicochem. Eng. Asp.* **2021**, *609*, 125663.
[12] S. Kushwaha, M. Mane, S. Ravindranathan, A. Das, *ACS Sens.* **2020**, *5*, 3254.
[13] Y. Wang, J. Xue, G. Nie, X. Guo, *Chem. Phys. Lett.* **2020**, *750*, 137444.
[14] Y. G. Park, S. N. Nam, M. Jang, C. Min Park, N. Her, J. Sohn, J. Cho, Y. Yoon, *Sep. Purif. Technol.* **2022**, *288*, 120637.
[15] P. Zhang, Y. Chen, Y. Chen, Q. Guo, Y. Liu, Y. Yang, Q. Cao, H. Chong, M. Lin, *Sci. Total Environ.* **2023**, *866*, 161378.
[16] Y. K. Recepoglu, A. Y. Goren, V. Vatanpour, Y. Yoon, A. Khataee, *Desalination* **2022**, *533*, 115782.

10974628, 0, Downloaded from https://onlinelibrary.wiley.com/doi/10.1002/app.54856 by Ali Bilici - Canakkale Onsekiz Mart Uni , Wiley Online Library on [09/11/2023]. See the Terms and Conditions (https://onlinelibrary.wiley.com/terms-and-conditions) on Wiley Online Library for rules of use; OA articles are governed by the applicable Creative Commons License

[17] J. Thomas, N. E. Weston, T. E. O'Connor, *J. Am. Chem. Soc.* **1962**, *84*, 4619.
[18] S. Yu, X. Wang, H. Pang, R. Zhang, W. Song, D. Fu, T. Hayat, X. Wang, *Chem. Eng. J.* **2018**, *333*, 343.
[19] E. Czarniewska, L. Mrówczyńska, M. Jędrzejczak-Silicka, P. Nowicki, M. Trukawka, E. Mijowska, *Sci. Rep.* **2019**, *9*, 14027.
[20] F. Lu, C. Liu, Z. Chen, U. Veerabagu, Z. Chen, M. Liu, L. Hu, H. Xia, L. Cha, W. Zhang, *Surf. Coat. Technol.* **2021**, *420*, 127273.
[21] P. Karthikeyan, S. S. D. Elanchezhiyan, J. Preethi, S. Meenakshi, C. M. Park, *Appl. Surf. Sci.* **2020**, *511*, 145543.
[22] M. Lu, *ChemistrySelect* **2021**, *6*, 3841.
[23] Z. Cai, X. Song, Q. Zhang, T. Zhai, *Fibers Polym.* **2017**, *18*, 502.
[24] A. Thadathil, H. Pradeep, D. Joshy, Y. A. Ismail, P. Periyat, *Mater. Adv.* **2022**, *3*, 2990.
[25] D. Devadathan, V. Baiju, J. P. Deepa, R. Raveendran, *Nanosyst. Phys. Chem. Math.* **2020**, *11*, 666.
[26] T. E. O'Connor, *J. Am. Chem. Soc.* **1962**, *84*, 1753.
[27] M. Wei, J. Liao, N. Liu, D. Zhang, H. Kang, Y. Yang, Y. Yang, J. Jin, *Nucl. Sci. Tech.* **2007**, *18*, 287.
[28] H. Zheng, L. Zhou, Z. Liu, Z. Le, J. Ouyang, G. Huang, H. Shehzad, *Micropor. Mesopor. Mater.* **2019**, *279*, 316.
[29] M. N. Khan, A. Sarwar, *Surf. Rev. Lett.* **2007**, *14*, 461.
[30] G. Newcombe, R. Hayes, M. Drikas, *Colloids Surf. A Physicochem. Eng. Asp.* **1993**, *78*, 65.
[31] M. Karegar, M. M. Khodaei, *Polym. Bull.* **2022**, *79*, 11431.
[32] B. Singh, G. Kaur, P. Singh, K. Singh, B. Kumar, A. Vij, M. Kumar, R. Bala, R. Meena, A. Singh, A. Thakur, A. Kumar, *Sci. Rep.* **2016**, *6*, 35535.
[33] V. Ugraskan, E. Ceran, O. Yazici, *Polym. Polym. Compos.* **2019**, *2021*, 1227.
[34] S. Shahabuddin, R. Khanam, M. Khalid, N. M. Sarih, J. J. Ching, S. Mohamad, R. Saidur, *Arabian J. Chem.* **2018**, *11*, 1000.
[35] K. Phasuksom, A. Sirivat, *Synth. Met.* **2016**, *219*, 142.
[36] A. Thadathil, J. Kavil, G. R. Kovummal, C. P. Jijil, P. Periyat, *ACS Omega* **2022**, *7*, 11473.
[37] G. Tang, X. Hou, Y. Wang, Z. Yan, T. Ren, L. Ma, X. Huang, C. Wang, *ACS Appl. Nano. Mater.* **2022**, *5*, 361.
[38] T. Jähnichen, J. Hojak, C. Bläker, C. Pasel, V. Mauer, V. Zittel, R. Denecke, D. Bathen, D. Enke, *ACS Omega* **2022**, *7*, 33375.
[39] P. Chhattise, K. Handore, A. Horne, K. Mohite, S. Dallavalle, S. Dallavalle, V. Chabukswar, *J. Chem. Sci.* **2016**, *128*, 467.
[40] B. Gupta, D. S. Chauhan, R. Prakash, *Mater. Chem. Phys.* **2010**, *120*, 625.
[41] S. Alkoy, C. Toy, T. Gönül, A. Tekin, *J. Eur. Ceram. Soc.* **1997**, *17*, 1415.
[42] E. Budak, Ç. Bozkurt, *Phys. B Condens. Matter* **2010**, *405*, 4702.
[43] C. J. Verma, A. S. Keshari, P. Dubey, R. Prakash, *Vacuum* **2020**, *177*, 109363.
[44] G. Rajasudha, D. Rajeswari, B. Lavanya, R. Saraswathi, S. Annapoorni, N. C. Mehra, *Colloid Polym. Sci.* **2005**, *283*, 575.
[45] S. Ahmad, A. Sultan, W. Raza, M. Muneer, F. Mohammad, *J. Appl. Polym. Sci.* **2016**, *133*, 133.
[46] G. Konwar, S. Deka, D. Mahanta, *J Energy Storage* **2023**, *62*, 106847.
[47] J. Qu, Q. Li, C. Luo, J. Cheng, X. Hou, *Coatings* **2018**, *8*, 214.
[48] K. S. W. Sing, R. T. Williams, *Adsorp. Sci. Technol.* **2004**, *22*, 773.
[49] M. Thommes, K. Kaneko, A. V. Neimark, J. P. Olivier, F. Rodriguez-Reinoso, J. Rouquerol, K. S. W. Sing, *Pure Appl. Chem.* **2015**, *87*, 1051.
[50] R. H. Müller, *Zetapotential und Partikelladung in der Laborpraxis*, Vol. 37, Wissenschaftliche Verlagsgesellschaft mbH, Stuttgart, Germany **1996**.
[51] I. M. Mahbubul, *Preparation, Characterization, Properties and Application of Nanofluid*, Elsevier, Oxford **2019**, p. 47.
[52] M. Marciniak, J. Goscianska, M. Norman, T. Jesionowski, A. Bazan-Wozniak, R. Pietrzak, *Materials* **2022**, *15*, 5573.
[53] P. Lai, H. Zhou, Z. Niu, L. Li, W. Zhu, L. Dai, *Chem. Eng. J.* **2023**, *457*, 141255.
[54] X. Yi, Z. Xu, Y. Liu, X. Guo, M. Ou, X. Xu, *RSC Adv.* **2017**, *7*, 6278.
[55] E. G. Sogut, D. Emre, A. Bilici, N. Caliskan Kilic, S. Yilmaz, *Mater. Chem. Phys.* **2022**, *290*, 290.
[56] J. Li, S. He, R. Li, W. Dai, J. Tao, C. Wang, J. Liu, T. Wu, C. Tang, *RSC Adv.* **2018**, *8*, 32886.
[57] Z. Yin, D. Pan, P. Li, P. Liu, H. Wu, W. Wu, *Radiochim. Acta* **2018**, *106*, 559.
[58] S. Y. Lagergreen, *Zeitschrift für Chemie Und Industrie der Kolloide* **1907**, *2*, 15.
[59] Y. S. Ho, G. McKay, *Process Biochem.* **1999**, *34*, 451.
[60] W. J. Weber, J. C. Morris, *J. Sanit. Eng. Div. Am. Soc. Civ. Eng.* **1963**, *89*, 31.
[61] D. Robati, *J. Nanostruct. Chem.* **2013**, *3*, 55.
[62] S. Azizian, *J. Colloid Interface Sci.* **2004**, *276*, 47.
[63] F.-C. Wu, R.-L. Tseng, R.-S. Juang, *Chem. Eng. J.* **2009**, *153*, 1.
[64] H. Freundlich, *Zeitschrift für Physikalische Chemie* **1907**, *57U*, 385.
[65] I. Langmuir, *J. Am. Chem. Soc.* **1918**, *40*, 1361.
[66] O. Redlich, L. Peterson, *J. Phys. Chem.* **1959**, *63*, 1024.
[67] M. M. Dubinin, L. V. Radushkevich, *Proc. Acad. Sci. USSR Chem. Sec.* **1947**, *55*, 331.
[68] F.-C. Wu, B.-L. Liu, K.-T. Wu, R.-L. Tseng, *Chem. Eng. J.* **2010**, *162*, 21.
[69] R. E. Treybal, *Mass-Transfer Operations*, McGraw-Hill, New York, NY **1981**.
[70] G. McKay, H. S. Blair, J. R. Gardner, *J. Appl. Polym. Sci.* **1982**, *27*, 3043.
[71] L. R. Bonetto, F. Ferrarini, C. de Marco, J. S. Crespo, R. Guégan, M. Giovanela, *J. Water Process Eng.* **2015**, *6*, 11.
[72] T. S. Singh, K. K. Pant, *Sep. Purif. Technol.* **2004**, *36*, 139.
[73] EPA, Radionuclides notice of data availability technical support document; Washington, DC (2000).
[74] M. F. Cheira, *Int. J. Environ. Anal. Chem.* **2021**, *101*, 1710.
[75] Z. Abdeen, Z. F. Akl, *RSC Adv.* **2015**, *5*, 74220.
[76] E. Broda, A. Gładysz-Płaska, E. Skwarek, V. V. Payentko, *Appl. Nanosci.* **2022**, *12*, 1101.
[77] K. Li, T. Xiong, J. Liao, Y. Lei, Y. Zhang, W. Zhu, *Chem. Eng. J.* **2022**, *433*, 134449.
[78] H. H. El-Maghrabi, A. A. Younes, A. R. Salem, K. Rabie, E. El-shereafy, *J. Hazard. Mater.* **2019**, *378*, 120703.
[79] P. Atkins, J. de Paula, *Physical Chemistry*, 8th ed., W. H. Freeman and Company, New York, NY **2006**.
[80] R. E. Dickerson, I. Geis, *Chemistry, matter, and the universe: An integrated approach to general chemistry*, W.A. Benjamin Inc, Menlo Park, CA **1976**.
[81] H. Wei, H. Wang, A. Li, D. Cui, Z. Zhao, L. Chu, X. Wei, L. Wang, D. Pan, J. Fan, Y. Li, J. Zhang, C. Liu, S. Wei, Z. Guo, *ChemNanoMat* **2020**, *6*, 174.

10974628, 0, Downloaded from https://onlinelibrary.wiley.com/doi/10.1002/app.54856 by Ali Bilici - Canakkale Onsekiz Mart Uni , Wiley Online Library on [09/11/2023]. See the Terms and Conditions (https://onlinelibrary.wiley.com/terms-and-conditions) on Wiley Online Library for rules of use; OA articles are governed by the applicable Creative Commons License

[82] K. K. Kefeni, B. B. Mamba, T. A. M. Msagati, *Sep. Purif. Technol.* **2017**, *188*, 399.
[83] D. Shao, G. Hou, J. Li, T. Wen, X. Ren, X. Wang, *Chem. Eng. J.* **2014**, *255*, 604.
[84] P. Zhang, Y. Chen, Q. Guo, Y. Liu, H. Chong, H. Weng, X. Zhao, Y. Yang, M. Lin, *Sep. Purif. Technol.* **2023**, *305*, 122538.
[85] M. Jansson-Charrier, E. Guibal, J. Roussy, R. Surjous, P. Le Cloirec, *Water Sci. Technol.* **1996**, *34*, 169.
[86] R. Say, A. Ersöz, A. Denizli, *Sep. Sci. Technol.* **2003**, *38*, 3431.
[87] T. S. Anirudhan, C. D. Bringle, S. Rijith, *J. Environ. Radioact.* **2010**, *101*, 267.

SUPPORTING INFORMATION

Additional supporting information can be found online in the Supporting Information section at the end of this article.

How to cite this article: D. Emre, Özlem Selçuk Zorer, A. Bilici, E. Budak, S. Yilmaz, N. C. Kilic, E. G. Sogut, *J. Appl. Polym. Sci.* **2023**, e54856. https://doi.org/10.1002/app.54856

10974628, 0, Downloaded from https://onlinelibrary.wiley.com/doi/10.1002/app.54856 by Ali Bilici - Canakkale Onsekiz Mart Uni , Wiley Online Library on [09/11/2023]. See the Terms and Conditions (https://onlinelibrary.wiley.com/terms-and-conditions) on Wiley Online Library for rules of use; OA articles are governed by the applicable Creative Commons License